Supplementary material: Discussion of the nuclear and electron dynamics underlying the pump-probe signals

In this section we discuss various aspects of the nuclear and electron dynamics and their interrelation to the pump-probe signals in greater detail. For simplicity, our discussion will be for the single NIR-probe pulse peak intensity $I_M = 5\times10^{13}$ Wcm^{-2} (i.e., without focal averaging), which constitutes an intermediate intensity in the laser focus spot and which was also used in Fig. 4 of the main text. Supplementary Fig. 1 shows the simulated average He charge $\langle q_{He}\rangle$ in panel (a) and the absorbed NIR laser energy W_{abs} in panel (b) for the $He_{2171}\cdot Ar_{13}$ system as functions of the pump-probe delay time Δt. The average He charge is defined as $\langle q_{He}\rangle = (N_1+2N_2)/(N_0+N_1+N_2)$, where N_0, N_1 and N_2 are the number of neutral He atoms, He^+ and He^{2+} ions at the end of a trajectory, respectively, without TBR correction. Both $\langle q_{He}\rangle$ and W_{abs} express the susceptibility of the x-ray-activated droplet for undergoing a laser-driven avalanche ionization for the given NIR pulse parameters.

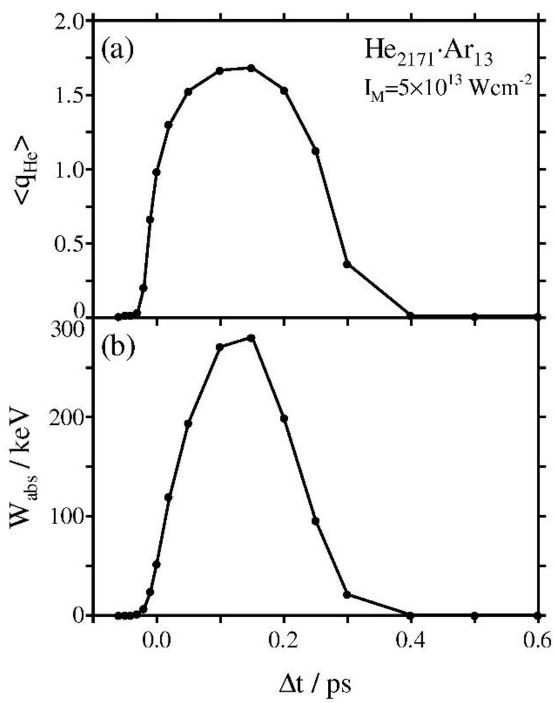

SM Figure 1. Pump-probe curves for $He_{2171}\cdot Ar_{13}$ for the NIR pulse peak intensity $I_M = 5\times10^{13}$ Wcm^{-2} without TBR correction and without focal averaging: (a) The average He charge $\langle q_{He}\rangle$ and (b) the energy W_{abs} absorbed from the NIR laser pulse.

To discuss the electron and nuclear dynamics at the onset of and during the arriving NIR probe pulse, Supplementary Fig. 2 shows a single-trajectory example of some key quantities of the $He_{2171}\cdot Ar_{13}$ system as a function of time t for the delay time Δt =150 fs which corresponds to the maximum of the pump-probe signal curve. Displayed is the time range -100 fs ≤ t ≤ 100 fs, where t = 0 constitutes the instant of the maximum of the NIR pulse envelope. The instantaneous x-ray ionization takes place at t = -150 fs and is outside of the displayed time range. Panel (a) shows the envelope of the Gaussian NIR pulse. In panel (b) the advancement of the droplet ionization is displayed in terms of $\langle q_{He}\rangle$. The droplet is largely ionized during the laser pulse, with $\langle q_{He} \rangle$ beginning to rise at t ≈ -40 fs and reaching a final value of 1.7. The main purpose of panel (c) is to monitor ignition by the number of He^{+} ions (black curve) and electrons (red) curve inside the droplet. Ignition is assigned to the instant where the He^{+} population (black curve) has a kink, which marks the beginning of its steep rise.

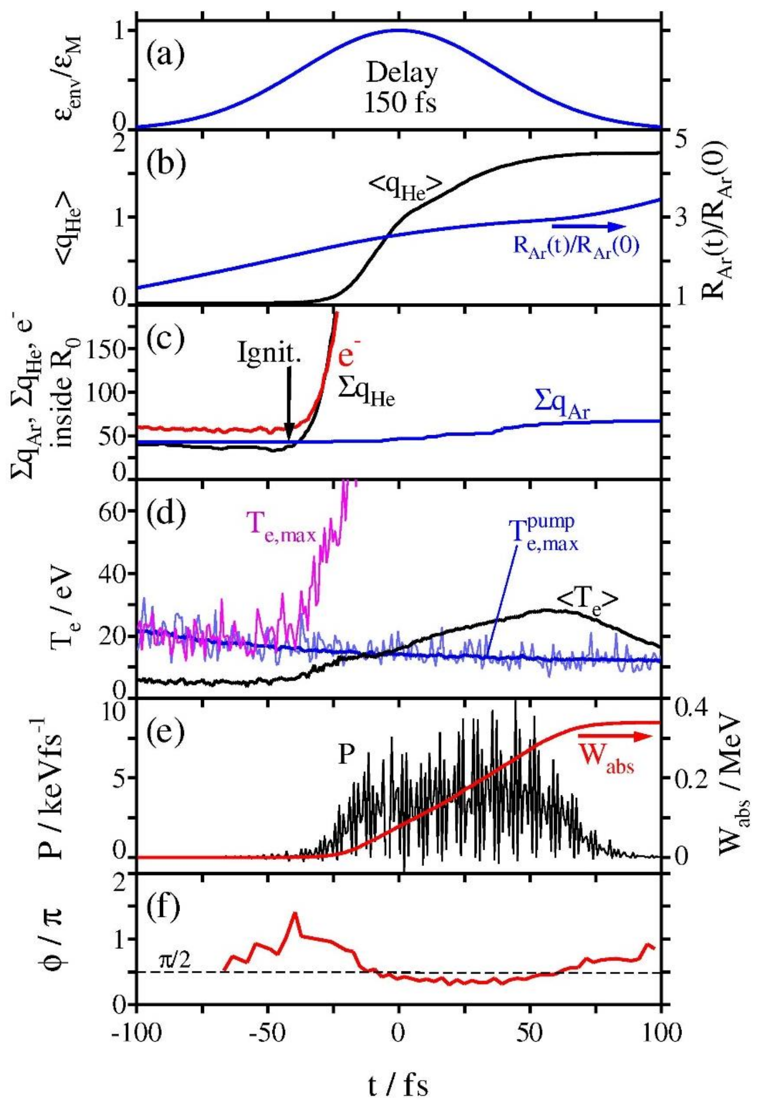

SM Figure 2. Single-trajectory example of the ionization dynamics of a $He_{2171}{\cdot}Ar_{13}$ droplet irradiated by a NIR pulse. The NIR pulse peak intensity is $I_M = 5{\times}10^{13}$ Wcm^{-2}, the pump-probe delay time 150 fs. The time axis refers to the maximum of the NIR pulse envelope. The instant of the x-ray-induced ionization is at t = -Δt = -150 fs and is outside the displayed time window. (a) The Gaussian electric field envelope of the NIR probe pulse, normalized to the electric field strength ε_M at the pulse peak maximum. (b) The average He charge $\langle q_{He} \rangle$ without TBR correction (black curve) and the radius of the expanding Ar_{13} cluster $R_{Ar}(t)$ relative to its initial radius $R_{Ar}(-\Delta t)$ before irradiation by the x-ray pulse (blue curve). $R_{Ar}(t)$ is taken as the average distance of the 12 Ar shell atoms from the central Ar atom of the Ar_{13} cluster. (c) The number of nanoplasma electrons (red curve), the number of He^+ atoms (black curve), and the sum of Ar^{q+} cation charges (blue curve) inside the unexpanded He_{2171} droplet (radius R_0 = 26.0Å). The instant of ignition is marked by the vertical arrow and is taken at the kink of the He^+ curve, from where the He ionization begins to rise markedly. In this single-trajectory example, the average Ar charge $\langle q_{Ar} \rangle$ amounts to 2.16 directly after the pump pulse, increases to 3.3 by secondary ionizations and reaches a final value of $\langle q_{Ar} \rangle$ = 5.2 after the NIR pulse (without TBR correction). (d) The maximum electron kinetic energy $T_{e,max}$ of a nanoplasma electrons inside the unexpanded droplet (magenta curve). For comparison, the maximum electron kinetic energy from a simulation without NIR pulse is given in two ways: A single-trajectory result $T_{e,max}^{(pump)}(t)$ (light blue curve) corresponding to the magenta energy $T_{e,max}$ curve, and the average $\langle T_{e,max}^{(pump)} \rangle(t)$ over 100 trajectories (bold dark blue curve), in which the fluctuations are smoothed out. (e) The power absorption P (black curve) and energy absorption W_{abs} (red curve) of the nanoplasma. (f) The phase ϕ between the COM of the nanoplasma electron cloud and the driving force exerted by the laser electric field. The dashed horizontal line marks the π/2 resonance value.

Panel (d) displays electron kinetic energies. Most interesting are the electrons in the high-energy tail of the kinetic energy distribution inside the droplet, since they have the best chances to overcome the Coulomb barriers at the He atoms and to trigger an EII avalanche. For simplicity, we only show the maximum energy $T_{e,max}$ as a representative of the high-energy tail, displayed by the magenta curve. To demonstrate the effect of the NIR pulse on $T_{e,max}$, the magenta $T_{e,max}(t)$ curve is compared with the corresponding single-trajectory result $T_{e,max}^{(pump)}(t)$ in which only the x-ray pump pulse is applied, i.e., without NIR probe pulse (light blue curve). To display also the smoothed base level of $T_{e,max}^{(pump)}(t)$ without fluctuations, a trajectory-set average over 100 trajectories, $\langle T_{e,max}^{(pump)} \rangle(t)$, is included as the bold dark blue curve. In the time interval t ≈ -70 to -40 fs, i.e., at the rising edge of the NIR pulse, prior to ignition, both fluctuations and level of the magenta curve are considerably above the blue $T_{e,max}^{(pump)}(t)$ and $\langle T_{e,max}^{(pump)} \rangle(t)$ curves, where the peaks of $T_{e,max}^{(pump)}(t)$ reach up to almost 35 eV. Without NIR pulse, $\langle T_{e,max}^{(pump)} \rangle(t)$ (bold dark blue curve) continuously decreases with time due to the expansion of the dopant cluster and due the escape of energetic electrons from the droplet. We attribute the differences between the magenta and the blue curves to the enhancement by the ion-assisted electron acceleration mechanism [1].

We consider the kinetic energy enhancement as a considerable contribution to ignition, as the electron kinetic energy peaks are in the range 20-35 eV. This indicates the enhancement of the high energy tail of the nanoplasma electron kinetic energy distribution, exceeding the Coulomb barriers of neutral He atoms which are downshifted to 8-20 eV with a few of them even down to 5 eV.

During the EII avalanche, $T_{e,max}$ reaches up to almost 300 eV and is outside the displayed energy range. For comparison, the average electron kinetic energy reaches only 30 eV during the EII avalanche (black curve). It is interesting to note that in the time range ≈ -70 to -40 fs, when the droplet is about to undergo ignition, the Ar_{13} cluster radius has expanded by a factor of 1.7 to 2.1 of its initial value of 3.76 Å (blue curve in panel (b)). Thus, despite this spatial expansion, the Ar_{13} cluster is apparently still sufficiently compact to assist the electron acceleration by the laser field. As Saalmann and Rost [1] showed for a rectangular model potential of depth ΔV, the electron kinetic energy enhancement is $\propto\sqrt{\Delta V}$ and $\propto\varepsilon$ (ε being the laser electric field strength). Thus, a more compact Ar_{13} cluster would be desirable, but which is realized only at earlier times when the laser field is still weak.

Panel (e) displays the strong NIR laser power absorption P (black curve) and energy absorption W_{abs} (red curve) during the EII avalanche. The resonant nature of the power and energy absorption is documented in panel (f) by the phase ϕ between the amplitudes of the force exerted on the electrons by the oscillating NIR laser electric field and the amplitudes of the center of mass (COM) of the nanoplasma electron cloud [2]. Prior to ignition (cf. the instant of ignition marked in panel (c)), ϕ assumes values around π. Only after ignition, ϕ drops and passes the resonance value $\pi/2$. Although ϕ subsequently further drops to values 0.3π-0.4π during the largest part of the EII avalanche, laser energy absorption remains high and, in view of the strong damping prevailing in nanoplasmas [2], the system is effectively close to resonance. Towards the end of the EII avalanche, ϕ passes again $\pi/2$ and tends to the value of π in the shallow potential well of the spatially expanded nanoplasma. Thus, the avalanche EII exhibits the typical resonance behavior which is known from previous EII avalanches in He nanoplasmas. We note that the given example clearly shows that ignition occurs first and resonance only subsequently. That is to say, it is not the case that relatively few electrons resonate first and this then causes ignition.

To show the resonance behavior of the $He_{2171}\cdot Ar_{13}$ droplet across the pump-probe delay time range, Supplementary Fig. 3 exhibits the phase ϕ for eight delay times, for ten trajectories per delay time. For comparison, the normalized oscillating electric field of the NIR pulse is given in the uppermost panels. The typical resonance behavior discussed in panel (f) of Supplementary Fig. 2, i.e., ϕ starting with values of $\approx\pi$, dropping down to $\pi/3$ during near resonance and then rising again towards the end of the EII avalanche, becomes apparent for $\Delta t \geq$ -10 fs (panel (c)). With increasing delay time, the first passage of the $\pi/2$ line is shifted to earlier times during the NIR pulse, as ignition occurs at earlier instants. The earlier ignition takes place during the pulse, the longer the pulse can drive the EII avalanche near-resonantly. The longest near-resonant period is observed at Δt = 150 fs (panel (h)), i.e., at the maximum of the pump-probe signal curve. For Δt = 200 fs (panel (i)), the first π/2 passage is shifted again to later instants around the pulse peak maximum, reflecting the decreased activation state of the droplet. At Δt = 400 fs no ignition takes place, and the few generated nanoplasma electrons are driven in the shallow potential mainly of the ionized expanding Ar_{13} cluster. For Δt = -20 fs (panel (b)), the NIR pulse is effectively so much truncated that collective nanoplasma electron oscillations occur at most for only a very short time period towards the end of the laser pulse. Thus, it is the activation state of the droplet and/or NIR pulse truncation in the first place which determines the extent of a nanoplasma resonance.

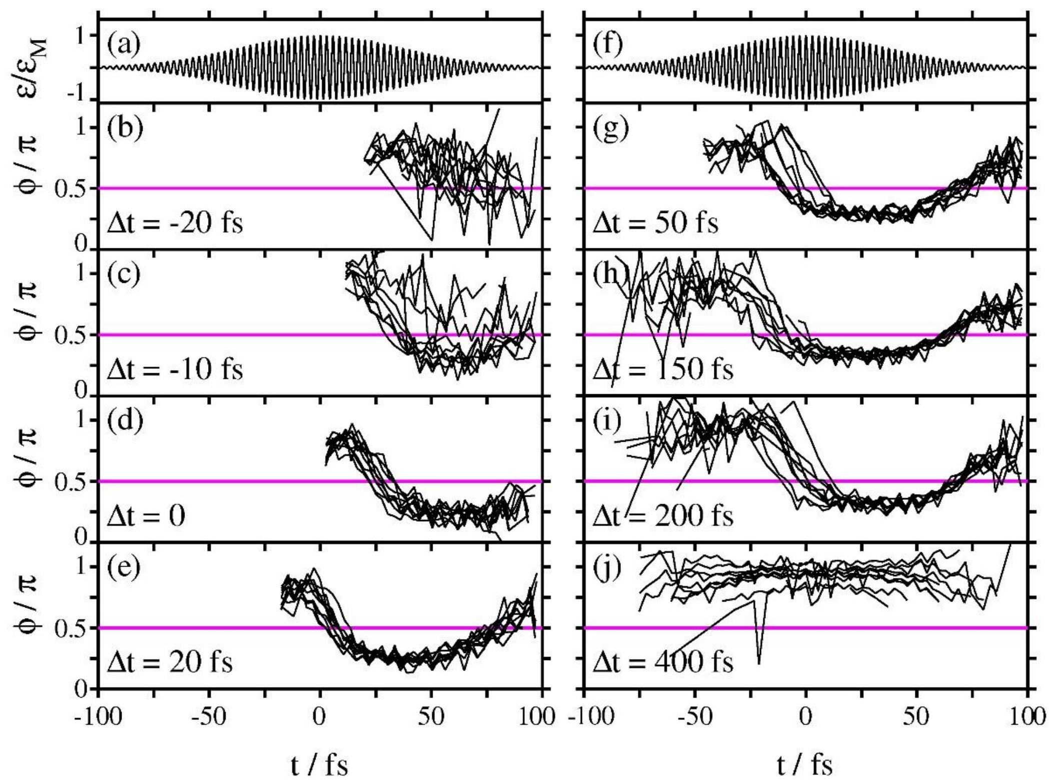

SM Figure 3. The resonance behavior of the $He_{2171}{\cdot}Ar_{13}$ system for eight different pump-probe delay times, represented by the phases ϕ between center-of-mass of the nanoplasma electron cloud and the driving force of the of the laser electric field. For each delay time, the phases of ten trajectories are given. Like in Supplementary Figure 2, the NIR pulse peak intensity is 5×10^{13} Wcm^{-2}. The magenta horizontal line marks the π/2 resonance value. For comparison, the oscillating laser electric field, normalized to the value at the pulse peak maximum, is given in panels (a) and (f).

Supplementary Fig. 4 shows the dopant cluster size dependence of $\phi(t)$ for the He_{2171} droplet doped with Ar_8, Ar_{13} and Ar_{23}. With increasing the dopant cluster size, the instant of ignition is shifted to earlier times with the nanoplasma resonances becoming more extended and more pronounced. This is completely in line with what was stated in the discussion of Supplementary Fig. 3, given that the x-ray pump pulse ionizes all Ar atoms, providing more electrons and cations from the Ar cluster and from the He shell and therefore leading faster to a sufficient activation of the droplet to trigger an EII avalanche.

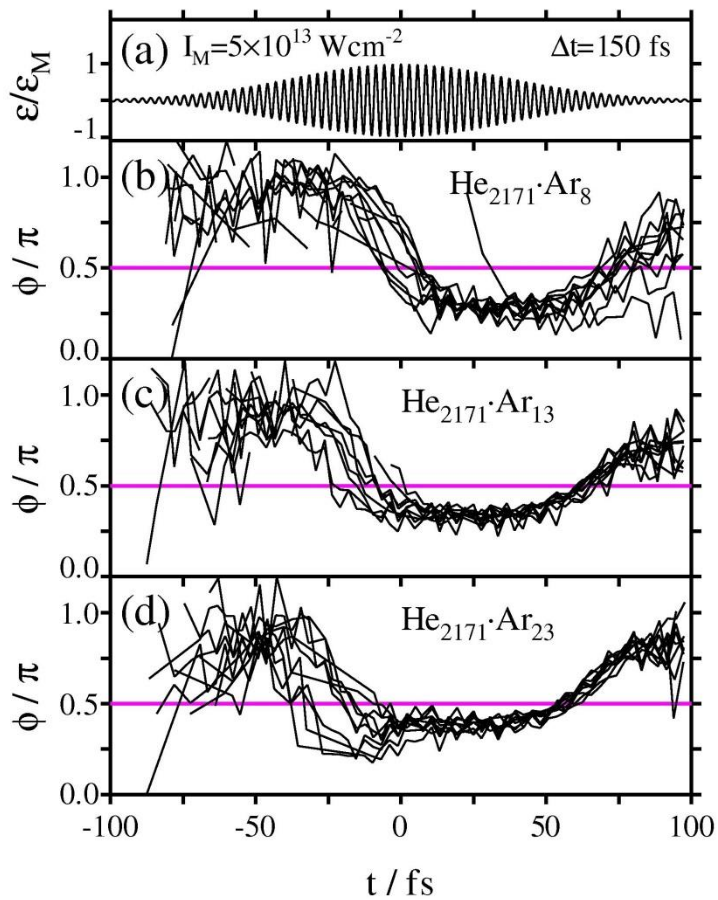

SM Figure 4. The dopant cluster size dependence of the resonance behavior. Each for the maximum of the pump-probe signal curves at Δt = 150 fs, the phases of 10 trajectories of the He_{2171} droplet doped with an Ar_8, Ar_{13} and Ar_{23} cluster are shown. The NIR pulse peak intensity is 5×10^{13} Wcm^{-2}.

References

[1] U. Saalmann and J. M. Rost, Phys. Rev. Lett. **100**, 133006 (2008).

[2] U. Saalmann and J. M. Rost, Phys. Rev. Lett. **91**, 223401 (2003).